13th World Conference on Earthquake Engineering
Vancouver, B.C., Canada
August 1-6, 2004
Paper No. 2446

NONLINEAR ANALYSIS OF CFT SUBJECTED TO COMBINED AXIAL COMPRESSIVE FORCE AND MOMENT

H.-T. HU[1], C.-S. HUANG[2] and Z.-L. CHEN[3]

SUMMARY

Proper material constitutive models for concrete-filled tube (CFT) columns subjected to combined axial force and bending moment are proposed and verified by the nonlinear finite element program ABAQUS against experimental data. The cross sections of the CFT columns in the numerical analysis are categorized into three groups, i.e., circular section, square section, and square section stiffened by reinforcing ties. Via the numerical analyses, it is shown that the steel tubes can provide a good confining effect to the concrete core when the axial compressive force is large. The confining effect of square CFT stiffened by reinforcing ties is stronger than that of the same square CFT not stiffened with ties but weaker than that of circular section. When the spacing of reinforcing ties is small, the CFT with square section might possible achieve the same confining effect as that with circular section.

INTRODUCTION

Concrete-filled tube (CFT) column consists of a steel tube filled with concrete. The concrete fill adds stiffness and compressive strength to the tubular column and reduces the potential for inward local buckling. The steel tube acts as longitudinal and lateral reinforcement for the concrete core to resist tension, bending moment and shear, and to prevent the concrete from spalling. Due to the beneficial composite action of both materials, the CFT columns provide excellent seismic resistant structural properties such as high strength, high ductility and large energy absorption capacity. In addition, the steel tube acts as both erection steel and forming for the composite column during construction, thus decreasing a considerable amount of the labor and materials and reducing the construction cost. As a result, CFT columns have gained popularity in supporting heavy loads in high-rise buildings, bridges and offshore structures and various experimental and analytical studies have been performed on CFT columns such as Ge [1], Bradford [2], Schneider [3], Uy [4], Elremaily [5] and Hu [6].

It is known that the ultimate strengths of CFT columns are influenced by their constituent material properties such as the compressive strength of the concrete, the yield strength of the steel, and the nonlinear behaviors of these two materials. In addition, the ultimate strengths of CFT columns are also

[1] Professor, Dept. of Civil Eng., National Cheng Kung University, Tainan, Taiwan, R.O.C., E-mail: hthu@mail.ncku.edu.tw
[2] Professor, Dept. of Civil Eng., National Chiao Tng University, Hsinchu, Taiwan., R.O.C.
[3] Research Assistant, Dept. of Civil Eng., National Cheng Kung University, Tainan, Taiwan, R.O.C.

influenced by the concrete confining pressure and the geometric properties of the tubes such as the shape of the cross section and the spacing and the diameter of the reinforcing ties. Therefore, to predict the ultimate strengths of CFT columns accurately, those important issues have to be clearly understood. In this paper, proper nonlinear constitutive material models for steel reinforcing tie, steel tube and confined concrete are proposed. Then, the nonlinear finite element program ABAQUS [7] is employed to perform numerical simulations of CFT columns subjected to combined axial compressive forces and bending moments. The proposed material constitutive models are verified against experimental data of Liu et al. [8]. Finally, the influence of the concrete confining pressure and the geometric properties of the columns on the behavior of CFT columns are studied and discussed.

MATERIAL PROPERTIES AND CONSTITUTIVE MODELS

Material properties and constitutive models

The cross sections of the CFT columns in this investigation can be categorized into three groups (Fig. 1), i.e., circular section (denoted by CU), square section (denoted by SU), and square section stiffened with steel reinforcing ties forming an octagonal shape (denoted by SS). The materials used in the numerical analysis involve steel reinforcing tie (for SS section only), steel tube and concrete. Constitutive models of these materials are proposed and discussed as follows.

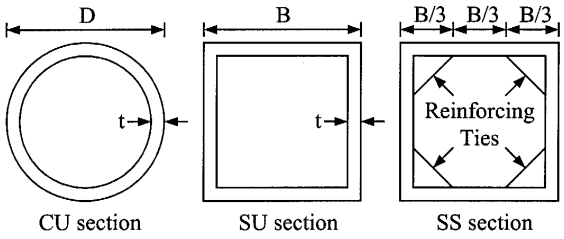

Fig. 1 Cross sections of CFT columns

Steel reinforcing tie

When the stress in the reinforcing tie exceeds the yield stress σ_y, the tie will exhibit plastic deformation. The stress-strain curve of the reinforcing tie is assumed to be elastic-perfectly plastic. The elastic modulus of the reinforcing tie E_S is assumed to be E_S = 200 GPa.

Steel tube

In the analysis, the Poisson's ratio ν_s and the elastic modulus E_S of the steel tube are assumed to be ν_s = 0.3 and E_S = 200 GPa. The uniaxial behavior of the steel tube is similar to reinforcing tie. When the steel tube is subjected to multiple stresses, a von Mises yield criterion is employed to define the elastic limit. The response of the steel tube is modeled by an elastic-perfectly-plastic theory with associated flow rule. When the stress points fall inside the yield surface, the behavior of the steel tube is linearly elastic. If the stresses of the steel tube reach the yield surface, the behavior of the steel tube becomes perfectly plastic. Consequently, the steel tube is assumed to fail and can not resist any further loading.

Concrete

In this study, the Poisson's ratio of concrete is assumed to be ν_c = 0.2. Let the uniaxial compressive strength and the corresponding strain of the unconfined concrete be f_c' and ε_c' (Fig. 2). The value of ε_c' is usually around the range of 0.002 to 0.003. A representative value ε_c' = 0.002 is used in the analysis. When concrete is subjected to laterally confining pressure, the uniaxial compressive strength f_{cc}' and the corresponding strain ε_{cc}' (Fig. 2) are much higher than those of unconfined concrete. The relations between f_{cc}', f_c' and between ε_{cc}', ε_c' are estimated by the following equations, Mander [9]:

$$f'_{cc} = k_4 f'_c + k_1 f_l, \qquad \varepsilon'_{cc} = \varepsilon'_c \left(1 + k_2 \frac{f_l}{f'_c}\right) \tag{1}$$

where f_l represents the confining pressure around the concrete core. The k_1 and k_2 are constants and can be obtained from experimental data. Meanwhile, the constants k_1 and k_2 were set as 4.1 and 20.5 based on the studies of Richart et al. [10]. The original equation of Eq. (1) is proposed for concrete subjected to hydrostatic pressure and does not contain the strength factor k_4. For CFT subjected to bending moment, part of the concrete may be subject to tensile stress, which is different from the hydrostatic pressure condition. Therefore, a strength factor k_4 is introduced by the authors with the limitation $k_4 \le 1$.

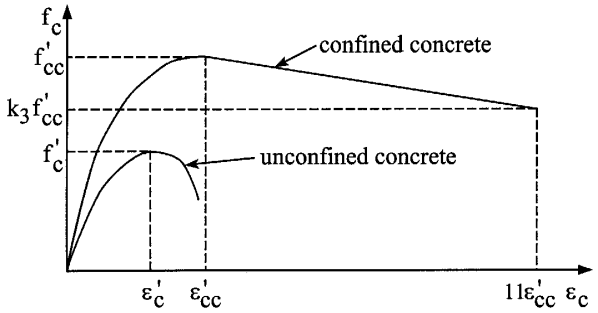

Fig. 2 Equivalent uniaxial stress-strain curve for concrete

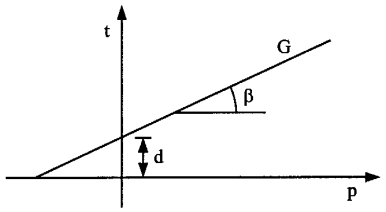

Fig. 3 Linear Drucker-Prager yield criterion for concrete

Because the concrete in the CFT columns is usually subjected to triaxial compressive stresses, the failure of concrete is dominated by the compressive failure surface expanding with increasing hydrostatic pressure. Hence, a linear Drucker-Prager yield criterion G (Fig. 3) is used to model the yield surface of concrete, which is expressed as

$$G = t - p\tan\beta - d = 0 \tag{2}$$

where

$$p = -(\sigma_1 + \sigma_2 + \sigma_3)/3, \qquad d = (1 - \frac{\tan\beta}{3}) f'_{cc}$$

$$t = \frac{\sqrt{3J_2}}{2}\left[1 + \frac{1}{K} - (1 - \frac{1}{K})\left(\frac{r}{\sqrt{3J_2}}\right)^3\right], \qquad r = \left[\frac{9}{2}(S_1^3 + S_2^3 + S_3^3)\right]^{1/3}$$

The σ_1, σ_2, and σ_3 are principal stresses and S_1, S_2, and S_3 are principal stress deviators. The constants K and β are material parameters determined from experimental data. In the analysis, K = 0.8 and $\beta = 20^O$ are used, Chen [11].

The response of the concrete is modeled by an elastic-plastic theory with associated flow and isotropic hardening rule. When plastic deformation occurs, there should be a certain parameter to guide the expansion of the yield surface. A commonly used approach is to relate the multidimensional stress and

strain conditions to a pair of quantities, namely, the effective stress f_c and effective strain ε_c, such that results obtained following different loading paths can all be correlated by means of the equivalent uniaxial stress-strain curve. The stress-strain relationship proposed by Saenz [12] has been widely adopted as the uniaxial stress-strain curve for concrete and it has the following form

$$f_c = \frac{E_c \varepsilon_c}{1 + (R + R_E - 2)(\frac{\varepsilon_c}{\varepsilon'_{cc}}) - (2R - 1)(\frac{\varepsilon_c}{\varepsilon'_{cc}})^2 + R(\frac{\varepsilon_c}{\varepsilon'_{cc}})^3} \tag{3}$$

where

$$R = \frac{R_E(R_\sigma - 1)}{(R_\varepsilon - 1)^2} - \frac{1}{R_\varepsilon} \quad , \qquad R_E = \frac{E_c \varepsilon'_{cc}}{f'_{cc}}$$

and $R_\sigma = 4$, $R_\varepsilon = 4$ may be used, Hu [13]. The initial modulus of elasticity of concrete E_c is highly correlated to its compressive strength and can be calculated with reasonable accuracy from the empirical equation, ACI [14]:

$$E_c = 4700\sqrt{f'_{cc}} \text{ MPa} \tag{4}$$

In the analysis, Eq. (3) is taken as the equivalent uniaxial stress-strain curve for concrete when the concrete strain ε_c is less than ε'_{cc} (Fig. 2). When $\varepsilon_c > \varepsilon'_{cc}$, a linear descending line is used to model the softening behavior of concrete. If k_3 is defined as the material degradation parameter, the descending line is assumed to be terminated at the point where $f_c = k_3 f'_{cc}$ and $\varepsilon_c = 11\varepsilon'_{cc}$. Generally, the parameters f_l, k_3 and k_4 should be provided in order to completely define the equivalent uniaxial stress-strain relation. These three parameters apparently depend on the cross-sectional shape and stiffening mean. Consequently, their appropriate values are determined by matching the numerical results with experimental data via parametric study.

FINITE ELEMENT MODEL FOR CFT COLUMNS

The tested CFT column is simply supported at two ends and is composed of a CFT at the center portion and two rigid steel beams with stiffeners at outer portions (Fig. 4a). The beam is compressed by a constant axial force F first. Then two concentrated lateral loads P, forming a four-point bending, are applied to the beam up to failure.

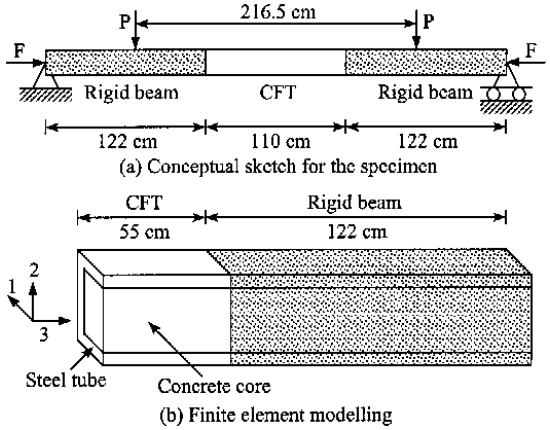

Fig. 4 Conceptual sketch and finite element modeling of CFT column

Due to symmetry, only one fourth of the CFT column is analyzed (Fig. 4b). Symmetric boundary

conditions are enforced on the symmetric planes, which are $u_3 = 0$ on the left surface of the element mesh and $u_1 = 0$ on the front surface of the element mesh surface. To simulate the roller support, the displacements u_2 for the nodes at the mid-depth of the right edge of the element mesh are all set to zero.

In the finite element mesh, both the concrete core and the steel tube are modeled by 27-node solid elements (three degrees of freedom per node) with reduced integration rule. For the SS section, the steel reinforcing tie is modeled by 3-node truss elements. The rigid portions of the beam are also modeled by 27-node solid elements. However, its material behavior is assumed to be linear elastic with elastic modulus $E_r = 1\times10^7$ GPa and Poisson's ratio $\nu_r = 0.01$. The interface between concrete core and steel tube is modeled by a pair of contact surfaces. The nodes of concrete core and steel tube are connected trough the contact surfaces that require matching meshes on the two bodies. The contact surfaces can model infinitesimal sliding and friction between concrete core and steel tube. The friction coefficient used in all the analyses is 0.25. Through the contact surfaces, concrete core and steel tube are allowed to either contact or separate but not to penetrate each other.

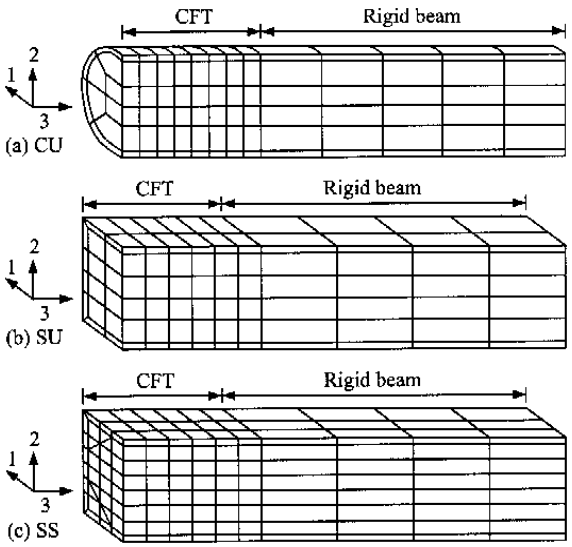

Fig. 5 Finite element meshes for CFT columns

Convergent studies of the finite element meshes have been done by the author using various element sizes for CFT columns with CU and SU sections, Chen [11]. It is shown that the results of these CFT columns are not sensitive to the element sizes and mesh refinement has very little influence on the numerical results. As the result, the meshes shown in Fig. 5 are used for CFT columns with CU, SU and SS sections through out the analyses.

NUMERICAL ANALYSIS

In this section, the experimental data from Liu et al. [8] are used to verify and calibrate the proposed material model for CFT columns. For convenience, each specimen in the analysis has an individual designation, involving two English letters followed by a series of numbers (Table 1). The first letter, C or S, represents the cross-sectional shape of the specimen to be circular or square, respectively. The second letter, S or U, denotes a specimen with or without stiffening ties, respectively. Meanwhile, the number following the English letters denotes the axial load ratio F/F_u of the beam, where F_u is the axial load strength calculated by using the Eurocode 4 [15]. For stiffened specimen, the last symbol, B/3 or B/5, represents the center-to-center spacing between the steel reinforcing ties and a unique size of tie bars (#3 bar with diameter 9.52 mm) is used.

Table 1 Geometry and material properties of CFT columns

Column No.	Axial Force F (kN)	D or B (mm)	t (mm)	D/t or B/t	Length (mm)	Steel Tube f_y (MPa)	Concrete f_c' (MPa)	Steel Tie f_y (MPa)
CU-0	0	280	4	70	1100	284.9	24.18	-
CU-0.21	542	280	4	70	1100	284.9	24.18	-
CU-0.31	812	280	4	70	1100	284.9	24.18	-
CU-0.41	1200	280	4	70	1100	287.7	29.07	-
CU-0.52	1354	280	4	70	1100	284.9	24.18	-
CU-0.68	2000	280	4	70	1100	287.3	29.07	-
SU-0	0	280	4	70	1100	284.9	24.18	-
SU-0.24	800	280	4	70	1100	287.3	29.07	-
SU-0.34	1035	280	4	70	1100	284.9	24.18	-
SU-0.35	1200	280	4	70	1100	287.3	29.07	-
SU-0.45	1378	280	4	70	1100	284.9	24.18	-
SU-0.57	1725	280	4	70	1100	284.9	24.18	-
SS-0-B/3	0	280	4	70	1100	284.9	24.18	407.6
SS-0.24-B/3	800	280	4	70	1100	287.7	29.07	467.5
SS-0.35-B/3	1200	280	4	70	1100	287.7	29.07	467.5
SS-0.47-B/3	1600	280	4	70	1100	287.7	29.07	467.5
SS-0.58-B/3	2000	280	4	70	1100	287.7	29.07	467.5
SS-0-B/5	0	280	4	70	1100	287.7	29.07	467.5
SS-0.24-B/5	800	280	4	70	1100	287.7	29.07	467.5
SS-0.35-B/5	1200	280	4	70	1100	287.7	29.07	467.5
SS-0.47-B/5	1600	280	4	70	1100	287.7	29.07	467.5
SS-0.58-B/5	2000	280	4	70	1100	287.7	29.07	467.5

Table 2 Results of numerical analyses

Column No.	Ultimate Moment (kN-m)		Error (%)	F_l (MPa)	f_l/f_y	k_3	k_4
	Experiment	Analysis					
CU-0	131.8	131.7	0.08	0.00	0.0000	1.00	0.70
CU-0.21	154.6	153.8	0.52	0.00	0.0000	0.93	1.00
CU-0.31	164.3	161.4	1.77	1.33	0.0047	0.75	1.00
CU-0.41	182.3	182.1	0.11	2.58	0.0090	0.65	1.00
CU-0.52	171.8	171.9	0.06	3.50	0.0123	0.55	1.00
CU-0.68	161.9	159.5	1.48	3.70	0.0129	0.61	1.00
SU-0	169.1	171.7	1.54	0.00	0.0000	0.87	0.47
SU-0.24	225.9	222.9	1.33	0.00	0.0000	0.63	0.88
SU-0.34	200.3	197.4	1.45	0.00	0.0000	0.55	0.97
SU-0.35	231.2	228.0	1.38	0.30	0.0010	0.50	1.00
SU-0.45	220.6	220.6	0.00	0.70	0.0025	0.47	1.00
SU-0.57	186.2	183.7	1.34	1.00	0.0035	0.46	1.00
SS-0-B/3	178.2	179.3	0.62	0.00	0.0000	0.93	0.50
SS-0.24-B/3	237.3	238.4	0.46	0.00	0.0000	0.88	0.90
SS-0.35-B/3	256.5	257.2	0.27	1.05	0.0036	0.70	1.00
SS-0.47-B/3	240.2	237.9	0.96	1.30	0.0045	0.35	1.00
SS-0.58-B/3	240.4	238.9	0.62	2.30	0.0080	0.35	1.00
SS-0-B/5	211.3	214.6	1.56	0.00	0.0000	1.00	0.70
SS-0.24-B/5	254.3	255.8	0.59	0.00	0.0000	0.96	0.93
SS-0.35-B/5	277.1	276.0	0.40	1.20	0.0042	0.90	1.00
SS-0.47-B/5	279.9	281.4	0.54	2.65	0.0092	0.68	1.00
SS-0.58-B/5	276.4	276.4	0.00	3.40	0.0118	0.55	1.00

Simulations of CFT columns with CU section

The results of numerical simulations for CFT columns with CU section are given in Table 2 and the curves of moment versus curvature at the midspan of the beams are plotted against the experiment data in Fig. 6. Generally, the numerical results show good agreement with the experimental data.

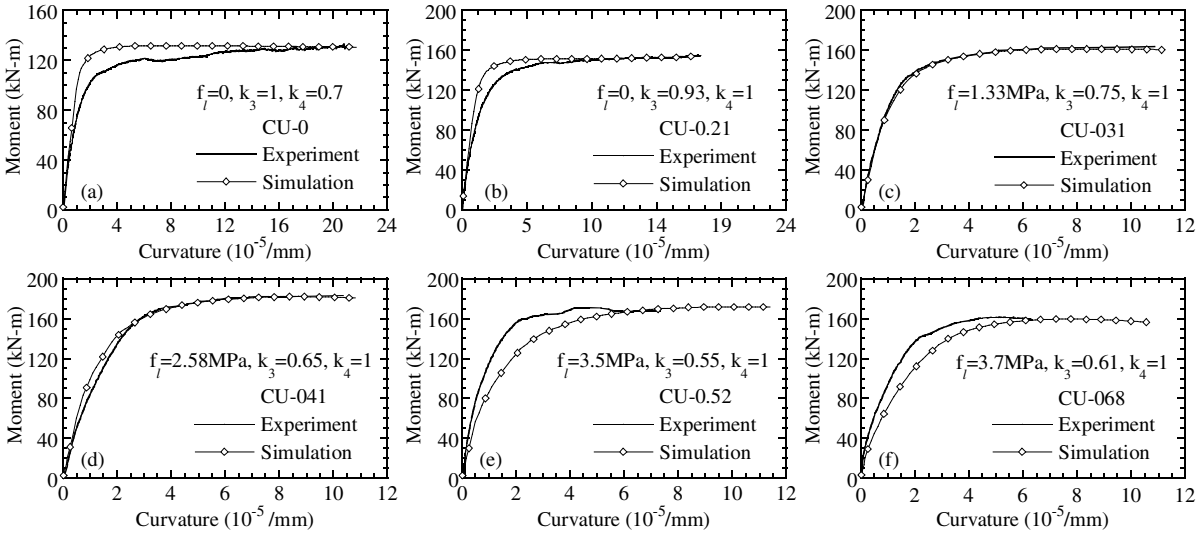

Fig. 6 Moment vs. curvature for CFT columns with CU section

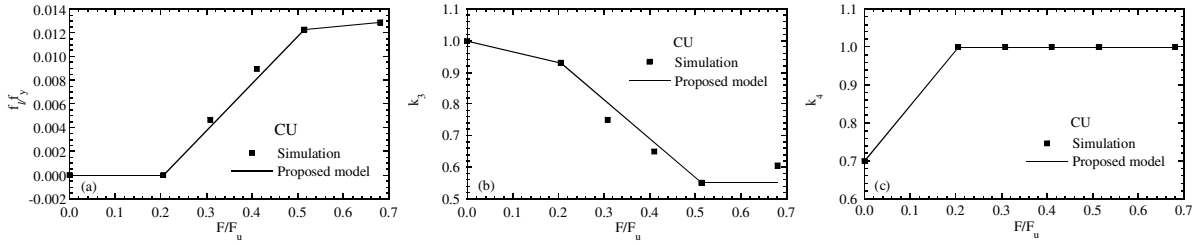

Fig. 7 f_l/f_y, k_3 and k_4 vs. axial load ratio F/F_u for CFT columns with CU section

Figures 7a, 7b and 7c show the values of f_l/f_y, k_3 and k_4 versus axial load ratio F/F_u for CFT columns with CU section, respectively. It can be observed from Fig. 7a that the axial load ratio F/F_u has significant influence on the lateral confining pressure f_l. When the axial load ratio F/F_u is less than 0.21, the steel tubes provide weak lateral support to the concrete core and the lateral confining pressure f_l applied to the concrete core is zero during the subsequent four-point bending loading. When the axial load ratio F/F_u is greater than 0.21, the steel tubes provide strong lateral support to the concrete core and the lateral confining pressure f_l increases with the increasing of axial load ratio F/F_u. However, when the axial load ratio F/F_u is greater than 0.52, the increasing of lateral confining pressure f_l is less sensitive to the F/F_u ratio. From the results of numerical simulations, the following empirical equations may be proposed for f_l/f_y as follows:

$$f_l / f_y = 0, \qquad 0 \le F/F_u \le 0.21 \tag{5a}$$

$$f_l / f_y = -0.00833 + 0.0397(F/F_u), \qquad 0.21 \le F/F_u \le 0.52 \tag{5b}$$

$$f_l / f_y = 0.0104 + 0.00375(F/F_u), \qquad 0.52 \le F/F_u \le 0.68 \tag{5c}$$

From Fig. 7b, we can see that the material degradation parameter k_3 generally decreases with the increasing of axial load ratio F/F_u. However, when the axial load ratio F/F_u is greater than 0.52, the

influence of F/F_u ratio on the parameter k_3 seems to be less significant. Based on the results of numerical simulations, the following empirical equations may be proposed for k_3 as follows:

$$k_3 = 1 - 0.342(F/F_u), \qquad 0 \le F/F_u \le 0.21 \tag{6a}$$

$$k_3 = 1.182 - 1.23(F/F_u), \qquad 0.21 \le F/F_u \le 0.52 \tag{6b}$$

$$k_3 = 0.55, \qquad 0.52 \le F/F_u \le 0.68 \tag{6c}$$

From Fig. 7c, we can see that the strength factor k_4 is less than 1 when the axial load ratio F/F_u is less than 0.21. This might mean when the axial compressive load is small, part of the concrete core is subjected to tensile stress during the four point bending. With weak later support from the steel tube, this part of concrete is prone to crack easily. On the average sense, the entire concrete cross section can not keep the strength f_c' and the strength factor k_4 is thus less than 1. When the axial compressive load is large (say $F/F_u > 0.21$), the concrete core has strong lateral support from the steel tube and is not prone to crack. As the result, the strength factor k_4 is set to the limit value 1. Based on the results of numerical simulations, the following empirical equations may be proposed for k_3 as follows:

$$k_4 = 0.7 + 1.463(F/F_u), \qquad 0 \le F/F_u \le 0.21 \tag{7a}$$

$$k_4 = 1, \qquad 0.21 \le F/F_u \tag{7b}$$

Figure 8a shows the typical deformation shapes of CU-0.31 column around the ultimate loading stage. It can be observed that the concrete core and steel tube still keep in contact to each other and no local buckling of the tube takes place. This phenomenon is also valid for CFT with CU section at other axial load ratios, Chen [11].

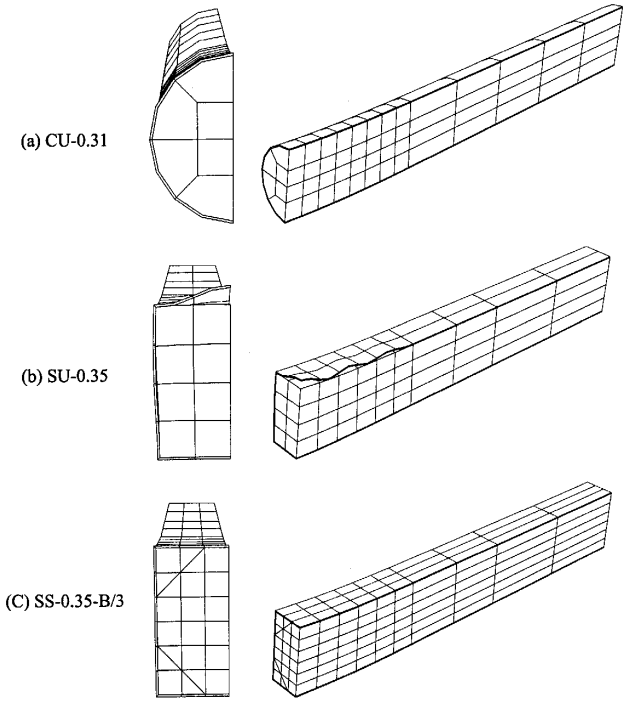

Fig. 8 Deformation shapes of CFT columns

Simulations of CFT columns with SU section

The results of numerical simulations for CFT columns with SU section are again given in Table 2 and the curves of moment versus curvature at the midspan of the beams are plotted against the experiment data in Fig. 9. Generally, the numerical results show good agreement with the experimental data.

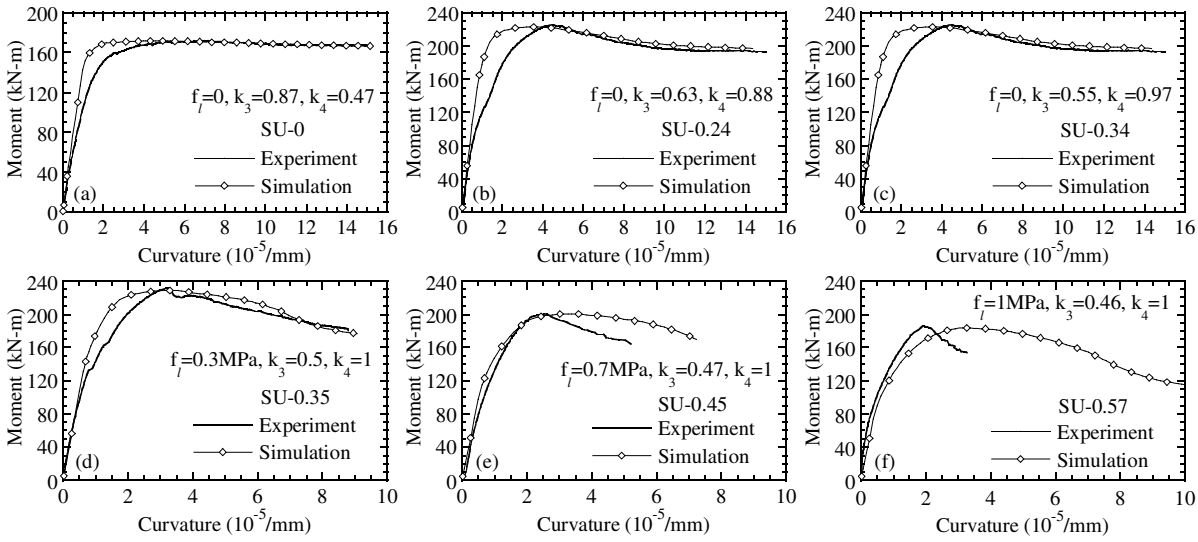

Fig. 9 Moment vs. curvature for CFT columns with SU section

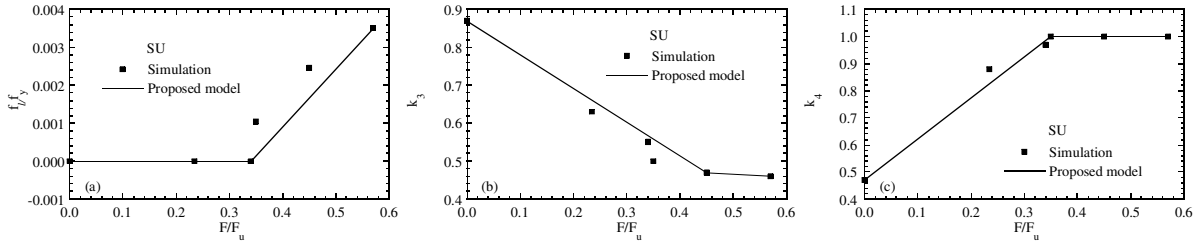

Fig. 10 f_l/f_y, k_3 and k_4 vs. axial load ratio F/F_u for CFT columns with SU section

Figures 10a, 10b and 10c show the values of f_l/f_y, k_3 and k_4 versus axial load ratio F/F_u for CFT columns with SU section, respectively. From Fig. 13a, we can see that when the axial load ratio F/F_u is less than 0.34, the lateral confining pressure f_l applied to the concrete core is zero. When the axial load ratio F/F_u is greater than 0.34, the steel tubes start to provide lateral support to the concrete core and the lateral confining pressure f_l increases with the increasing of axial load ratio F/F_u. Comparing Fig. 10a with Fig. 7a, one can observe that the lateral confining pressure f_l for CFT with SU section is much less than that with CU section. Even when the axial load ratio F/F_u is 0.57, the value of f_l/f_y ratio for CFT with SU section is only about 1/4 to that with CU section. From the results of numerical simulations, the following empirical equations may be proposed for f_l/f_y as follows:

$$f_l / f_y = 0, \qquad 0 \le F/F_u \le 0.34 \tag{8a}$$

$$f_l / f_y = -0.00517 + 0.0152(F / F_u), \qquad 0.34 \le F/F_u \le 0.57 \tag{8b}$$

From Fig. 10b, we can see again that the material degradation parameter k_3 decreases with increasing values of the axial load ratio F/F_u. When the axial load ratio F/F_u is greater than 0.45, the decreasing of the material degradation parameter k_3 is less sensitive to the F/F_u ratio. Comparing Fig. 10b with Fig. 7b, one can observe that the material degradation parameter k_3 for CFT with SU section is also smaller than that with CU section subjected to the same axial load ratio. This means that the strength of concrete in SU section degrades more than that in CU section. The reason can be explained as that the CFT tubes with SU section provide weaker lateral support to concrete core than those with CU section. From the results of numerical simulations, the following empirical equations may be proposed for k_3 as follows:

$$k_3 = 0.87 - 0.889(F/F_u), \qquad 0 \le F/F_u \le 0.45 \tag{9a}$$

$$k_3 = 0.508 - 0.083(F/F_u), \qquad 0.45 \le F/F_u \le 0.57 \tag{9b}$$

From Fig. 10c, we can see that the strength factor k_4 is less than 1 when the axial load ratio F/F_u is less than 0.35. Comparing Fig. 10c with Fig. 7c, we can see that with $F/F_u < 0.21$, the strength factor k_4 for CFT with SU section is usually smaller than that with CU section subjected to the same axial load ratio. This is again due to the CFT tubes with SU section provide weaker lateral support to concrete core than those with CU section. Based on the results of numerical simulations, the following empirical equations may be proposed for k_3 as follows:

$$k_4 = 0.42 + 1.706(F/F_u), \qquad 0 \le F/F_u \le 0.34 \tag{10a}$$

$$k_4 = 1, \qquad 0.34 \le F/F_u \le 0.57 \tag{10b}$$

Figure 8b shows the typical deformation shapes of SU-0.35 column during the ultimate loading stage. It can be observed that the concrete core and steel tube can not keep in contact to each other at the top and midspan region of the column where severe local buckling of the tube takes place. This phenomenon is also valid for CFT with SU section at other axial load ratios, Chen [11].

Simulations of CFT columns with SS section

The results of numerical simulations for CFT columns with SS section are given in Table 2 and the curves of axial force versus axial strain for these columns are plotted against the experiment data in Figs. 11 and 12. Generally, the numerical results again show good agreement with the experimental data.

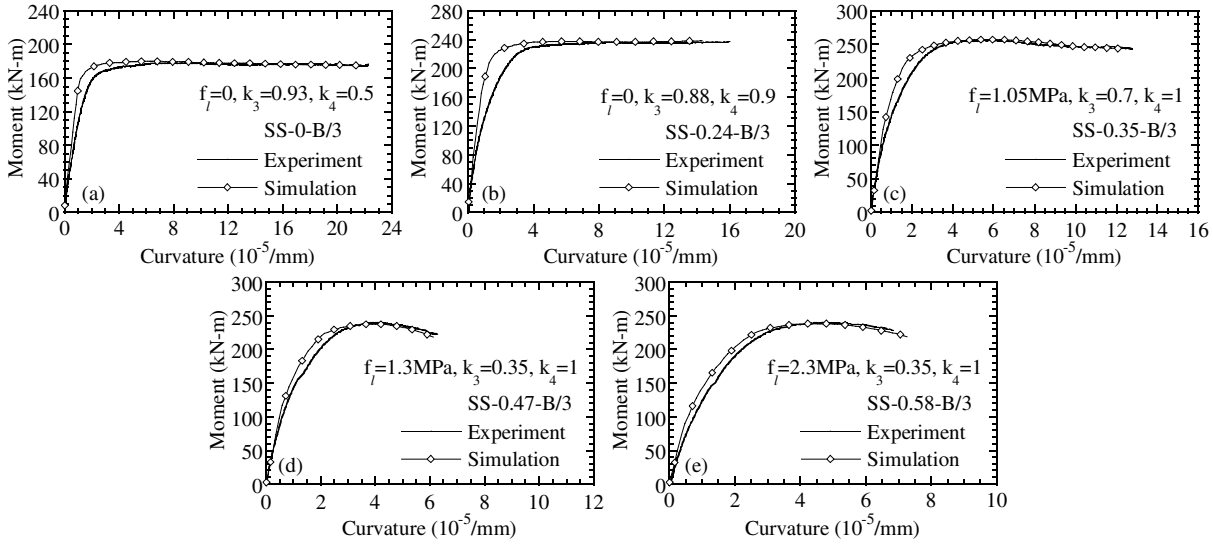

Fig. 11 Moment vs. curvature for CFT columns with SS-B/3 section

Figures 13a, 13b and 13c show the values of f_l/f_y, k_3 and k_4 versus axial load ratio F/F_u for CFT columns with SS section, respectively. From Fig. 13a, we can see that when the axial load ratio F/F_u is less than 0.24, the lateral confining pressure f_l applied to the concrete core is zero. When the axial load ratio F/F_u is greater than 0.24, the steel tubes start to provide lateral support to the concrete core and the lateral confining pressure f_l increases with the increasing of axial load ratio F/F_u. For CFT with reinforcing ties at close spacing (say B/5), its lateral confining pressure f_l is usually greater than that with reinforcing ties at large spacing (say B/3). Comparing Fig. 13a with Figs. 10a and 7a, one can observe that the lateral confining pressure f_l for CFT with SS section is much higher than that with SU section and is about the same order as that with CU section. This proves that the use of reinforcing ties enhances the lateral

confining pressure of the square tubes. From the results of numerical simulations, the following empirical equations may be proposed for f_l/f_y when reinforcing tie is at B/3 spacing:

$$f_l / f_y = 0, \qquad 0 \le F/F_u \le 0.24 \tag{11a}$$

$$f_l / f_y = -0.00565 + 0.0235(F / F_u), \qquad 0.24 \le F/F_u \le 0.58 \tag{11b}$$

When reinforcing tie is at B/5 spacing, the following equations may be suggested:

$$f_l / f_y = 0, \qquad 0 \le F/F_u \le 0.24 \tag{12a}$$

$$f_l / f_y = -0.00833 + 0.0347(F / F_u), \qquad 0.24 \le F/F_u \le 0.58 \tag{12b}$$

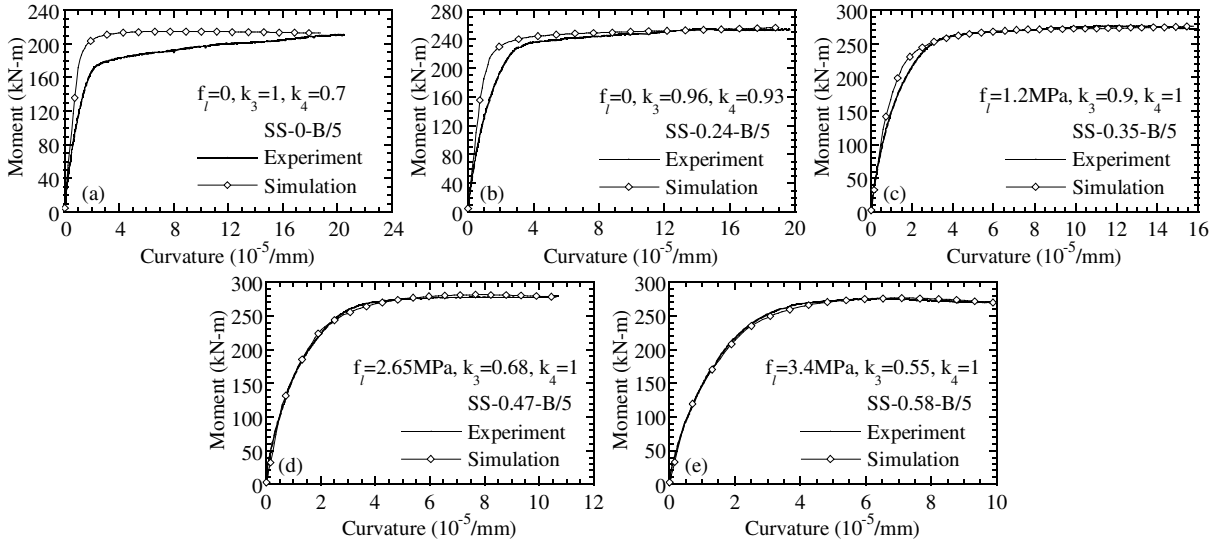

Fig. 12 Moment vs. curvature for CFT columns with SS-B/5 section

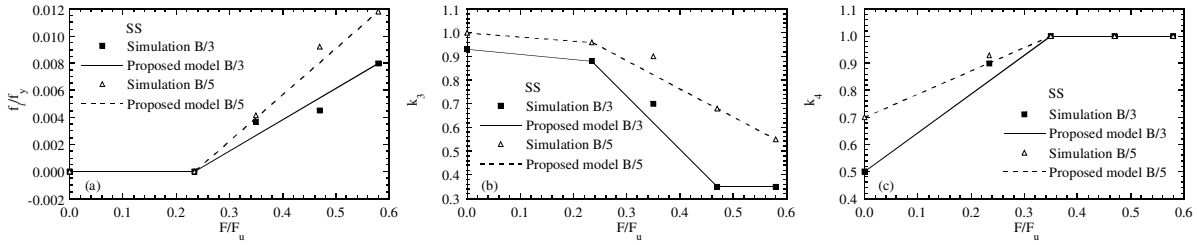

Fig. 13 f_l/f_y, k_3 and k_4 vs. axial load ratio F/F_u for CFT columns with SS section

From Fig. 13b, we can see again that the material degradation parameter k_3 decreases with increasing values of the axial load ratio F/F_u. For CFT with reinforcing ties at close spacing (say B/5), its material degradation parameter k_3 is usually greater than that with reinforcing ties at large spacing (say B/3) due to the enhancement of better lateral confining effect. Comparing Fig. 13b with Fig. 10b and7b, one can observe that with the same axial load ratio, the material degradation parameter k_3 for CFT with SS section is larger than that with SU section but smaller than that with CU section. However, when the spacing of reinforcing ties is small (say smaller than B/5), the CFT with SS section may possible keep up the same k_3 value as that with CU section. From the results of numerical simulations, the following empirical equations may be proposed for k_3 when reinforcing tie is at B/3 spacing:

$$k_3 = 0.93 - 0.214(F/F_u), \qquad 0 \le F/F_u \le 0.24 \tag{13a}$$

$$k_3 = 1.406 - 2.246(F/F_u), \qquad 0.24 \le F/F_u \le 0.47 \tag{13b}$$

$$k_3 = 0.35, \qquad 0.47 \le F/F_u \le 0.58 \tag{13c}$$

When reinforcing tie is at B/5 spacing, the following equations may be suggested:

$$k_3 = 1 - 0.17(F/F_u), \qquad 0 \le F/F_u \le 0.24 \tag{14a}$$

$$k_3 = 1.237 - 1.185(F/F_u), \qquad 0.24 \le F/F_u \le 0.58 \tag{14b}$$

From Fig. 13c, we can see that the strength factor k_4 is less than 1 when the axial load ratio F/F_u is less than 0.35. For CFT with reinforcing ties at close spacing (say B/5), its strength factor k_4 is usually greater than that with reinforcing ties at large spacing (say B/3). Comparing Fig. 13c with Fig. 10c and 7c, one can see that with the same axial load ratio, the strength factor k_4 for CFT with SS section is larger than that with SU section but smaller than that with CU section. However, when the spacing of reinforcing ties is small (say smaller than B/5), the CFT with SS section might possible maintain the same k_4 value as that with CU section. Based on the results of numerical simulations, the following empirical equations may be proposed for k_4 when reinforcing tie is at B/3 spacing:

$$k_4 = 0.5 + 1.429(F/F_u), \qquad 0 \le F/F_u \le 0.35 \tag{15a}$$

$$k_4 = 1, \qquad 0.35 \le F/F_u \le 0.58 \tag{15b}$$

When reinforcing tie is at B/5 spacing, the following equations may be suggested:

$$k_4 = 0.7 + 0.857(F/F_u), \qquad 0 \le F/F_u \le 0.35 \tag{16a}$$

$$k_4 = 1, \qquad 0.35 \le F/F_u \le 0.58 \tag{16b}$$

Figure 8c shows the typical deformation shapes of SS-0.35-B/3 column around the ultimate loading stage. It can be observed that the concrete core and steel tube again keep in contact to each other as the CFT with CU section. Due to the reinforcing ties, no local buckling of the tube takes place. This phenomenon is also valid for CFT with SS section at other axial load ratios and tie spacing [11].

CONCLUSIONS

Based on the numerical results, the following conclusions may be drawn:

(1) The lateral confining pressure f_l increases with the increasing of axial load ratio F/F_u. When this ratio is low, the steel tubes provide weak lateral support to the concrete core and the lateral confining pressure f_l applied to the concrete core may be zero during the subsequent four-point bending loading. When this ratio is high, the steel tubes provide strong lateral support to the concrete core.

(2) The lateral confining pressure f_l for CFT with SS section is much higher than that with SU section and is about the same order as that with CU section. The use of reinforcing ties enhances the lateral confining pressure of the tubes. For CFT with SS section, the lateral confining pressure f_l generally increases with the decreasing of tie spacing.

(3) For CFT with SU section, the concrete core and steel tube can not keep in contact to each other during the ultimate loading stage due to weak confining effect and severe local buckling of the tube takes place at the top and midspan region of the column. For CFT with CU and SS sections, local buckling is not likely to occur due to strong confining effect.

(4) The material degradation parameter k_3 generally decreases with the increasing of axial load ratio F/F_u. The material degradation parameter k_3 for CFT with SS section is larger than that with SU

section but smaller than that with CU section. However, when the spacing of reinforcing ties is small, the CFT with SS section may possible keep up the same k_3 value as that with CU section.

(5) When the axial load ratio F/F_u is low, the concrete cross section can not keep the strength f_c' on the average sense and the strength factor k_4 is smaller than 1. When the axial compressive load is large, the strength factor k_4 is equal to 1 due to strong confining effect. The strength factor k_4 for CFT with SS section is larger than that with SU section but smaller than that with CU section. When the spacing of reinforcing ties is small, the CFT with SS section might possible maintain the same k_4 value as that with CU section.

ACKNOWLEDGEMENTS

This research work was financially supported by the National Science Council, Republic of China under Grant NSC 90-2625-Z-006-007.

REFERENCES

1. Ge HB, Usami T. "Strength analysis of concrete-filled thin-walled steel box columns." Journal of Constructional Steel Research 1994;30(3):259-281.
2. Bradford MA. "Design strength of slender concrete-filled rectangular steel tubes." ACI Structural Journal 1996;93(2):229-235.
3. Schneider SP. "Axial loaded concrete-filled steel tubes. Journal of Structural Engineering 1998;124(10):1125-1138.
4. Uy B. "Strength of concrete filled steel box columns incorporating local buckling." Journal of Structural Engineering 2000;126(3):341-352.
5. Elremaily A, Azizinamini A. "Behavior and strength of circular concrete-filled tube columns." Journal of Constructional Steel Research 2002;58(12):1567-1591.
6. Hu H-T, Huang CS, Wu M-H, Wu Y-M. Nonlinear analysis of axially loaded CFT columns with confinement effect. Journal of Structural Engineering, ASCE, 2003;129(10):1322-1329.
7. Hibbitt, Karlsson & Sorensen, Inc., ABAQUS/Standard User Manuals, Version 6.2, Providence, Rhode Island, 2002.
8. Liu G-Y, Yeh Y-K, Huang CS, Tsai KC, Sun W-L. "A Study on the behaviors of concrete-filled steel tubular beam-columns under combined axial and bending loads." Research Report NCREE-00-008, National Center for Research on Earthquake Engineering, Taipei, Taiwan, R.O.C., 2000.
9. Mander JB, Priestley MJN, Park R. "Theoretical stress-strain model for confined concrete." Journal of Structural Engineering 1988;114(8):1804-1823.
10. Richart FE, Brandtzaeg A, Brown RL. "A study of the failure of concrete under combined compressive stresses." Bulletin 185, University of Illinois Engineering Experimental Station, Champaign, Illinois, 1928.
11. Chen Z-L. "Numerical analysis of concrete filled tubes subjected to combined axial force and moment." M.S. Thesis, Department of Civil Engineering, National Cheng Kung University, Tainan, Taiwan, R.O.C., 2001.
12. Saenz LP. Discussion of "Equation for the stress-strain curve of concrete" by Desayi P, Krishnan S., ACI Journal 1964;61:1229-1235.
13. Hu H-T, Schnobrich WC. "Constitutive modelling of concrete by using nonassociated plasticity." Journal of Materials in Civil Engineering 1989;1(4):199-216.
14. ACI Committee 318. "Building code requirements for structural concrete and commentary (ACI 318-99)."American Concrete Institute, Detroit, Michigan, 1999.
15. British Standards Institute. "Design of composite steel and concrete structure, Eurocode 4." London, 1994.